Testing Local Lorentz Invariance with Laser Tracking of the LAGEOS and LAGEOS II Satellites

David Lucchesi,[1,2,3,*] Massimo Visco,[1,2] Roberto Peron,[1,2] José C. Rodriguez,[4] Massimo Bassan,[5,2] Giuseppe Pucacco,[5,2] Luciano Anselmo,[3] Graham Appleby,[6] Marco Cinelli,[1,2] Alessandro Di Marco,[1,2] Marco Lucente,[1,2] Carmelo Magnafico,[1,2] Carmen Pardini,[3] and Feliciana Sapio[1,2]

(SaToR-G Collaboration)

[1]*Istituto Nazionale di Astrofisica (INAF), Istituto di Astrofisica e Planetologia Spaziali (IAPS), Via del Fosso del Cavaliere, 100, 00133 Roma, Italy*
[2]*Istituto Nazionale di Fisica Nucleare (INFN), Sezione di Tor Vergata, Via della Ricerca Scientifica 1, 00133 Roma, Italy*
[3]*Consiglio Nazionale delle Ricerche (CNR), Istituto di Scienza e Tecnologie della Informazione (ISTI), Via Giuseppe Moruzzi 1, 56124 Pisa, Italy*
[4]*Red de Infraestructuras Geodésicas, Instituto Geográfico Nacional, Madrid, Spain*
[5]*Dipartimento di Fisica, Università di Tor Vergata, Via della Ricerca Scientifica 1, 00133 Roma, Italy*
[6]*British Geological Survey, Herstmonceux Castle, Hailsham, United Kingdom*

(Received 28 November 2024; revised 20 March 2026; accepted 25 June 2026; published 27 July 2026)

Violations of Lorentz invariance, a cornerstone of modern physics, are predicted by theories of quantum gravity and by extensions of general relativity involving new vector or tensor fields. In the weak-field limit, such a violation would primarily manifest as a nonzero value for the post-Newtonian parameter α_1, which is identically zero in general relativity. We present a new test of local Lorentz invariance by searching for this signature in the orbits of the LAGEOS and LAGEOS II satellites. By applying a phase sensitive detection technique to the mean argument of latitude, derived from about 30 years of satellite laser ranging data, we isolate the periodic signal potentially induced by a preferred reference frame aligned with the cosmic microwave background. Our analysis yields a new constraint $|\alpha_1| \sim 2 \times 10^{-5}$. This result improves upon the previous best limit from lunar laser ranging and provides the most stringent constraint to date on preferred-frame effects in Earth's gravity.

DOI: 10.1103/v88p-965w

Introduction—Local lorentz invariance (LLI) states that the outcome of any local (in space and in time) nongravitational experiment is independent of the velocity of the freely falling apparatus in which the experiment is carried out. LLI represents a cornerstone in Einstein's theory of gravitation, general relativity (GR) [1], and, in particular, it represents one of the pillars of the Einstein equivalence principle (EEP) valid in GR and in all metric theories of gravity [2]. In GR, the only field that mediates the long-range gravitational interaction is the metric tensor $g_{\mu\nu}$. However, in the context of modern unification theories, other fields—scalar, vector, or tensor in their essence—may come to play a role in mediating the gravitational interaction in addition to the metric tensor of GR. In these unification theories, the action of a (four-)vector field K^{μ} or of other tensor fields $B_{\mu\nu}$, besides $g_{\mu\nu}$, is such that the distribution of matter in the universe typically selects a preferred rest frame for local gravitational physics and, consequently, implies a violation of LLI. Conversely, if only one or more scalar fields are present, besides the metric tensor $g_{\mu\nu}$, as in the case of tensor-multiscalar theories of gravitation [3], no violation of Lorentz invariance is expected. In the framework of the parameterized post-Newtonian (PPN) formalism [4–7], valid in the weak-field and slow-motion (WFSM) limit of GR, the preferred frame effects (PFE) are described by the parameters α_1, α_2, and α_3, that are all equal to zero in GR and in tensor-scalar theories of gravity. LLI and, consequently, PFE, are well tested in the context of high-energy physics experiments [8]—see also Ref. [9] for a review of Lorentz Invariance tests in effective field theories—but are much more difficult to test in the context of gravitation. Current best limits on LLI

*Contact author: david.lucchesi@inaf.it

obtained in the case of Solar System tests, i.e., in the WFSM limit of GR, were achieved [10,11] through lunar laser ranging (LLR) [12]: $\alpha_1 = (-7 \pm 9) \times 10^{-5}$ and $\alpha_2 = (+1.8 \pm 2.5) \times 10^{-5}$; and exploiting the close alignment between the spin of the sun and the total angular momentum of the solar system [13]: $|\alpha_2| \lesssim 2.4 \times 10^{-7}$. The above limits were obtained by assuming the existence of PFE with respect to the isotropic cosmic microwave background (CMB). In this Letter, under the same assumption, we provide a new constraint on the PPN parameter α_1 from the analysis of the orbital residuals of the geodetic satellites LAGEOS and LAGEOS II over a time interval of approximately 30 years. These are passive satellites very well tracked through the satellite laser ranging (SLR) technique [14,15]. In particular, we consider the possible existence of PFE due to the motion of the Earth-Sun-satellite system with respect to the CMB radiation and analyze the effect on the time evolution of a combination of Keplerian orbital parameters. To our knowledge, this is the first measurement that constrains the PPN parameter α_1 using artificial satellite orbits around the Earth. In an extended companion paper [16], details of the analyses performed to obtain the measurement are provided, along with an in-depth analysis of the main sources of systematic error and theoretical implications.

Orbital effects of PFE—In 1994, a seminal paper [17] suggested that the orbits of some artificial satellites have the potential to improve the upper limit on the α_1 parameter—down to the $\sim 10^{-6}$ level—thanks to the appearance of small divisors which enhance the corresponding PFE. This possibility of reaching a stringent constraint in the PPN parameter linked to the existence of possible PFE is mainly due to the precision of the SLR tracking technique, that allows to reconstruct the orbit of some geodetic satellites at the cm level. This is the case for the two LAGEOS satellites [18–21]. For these reasons their orbital reconstruction [22] has been exploited for fundamental physics measurements over three decades [23,24,27–35]. Starting from the Lagrangian $\mathcal{L}$ of $\mathcal{N}$ ideal proof masses gravitationally interacting, it can be shown that the dependency of $\mathcal{L}$ on the two PPN parameters α_1 and α_2 (if different from zero) will provide nonboost invariant terms depending on the velocities $\mathbf{v}_a^0$ of the proof masses with respect to some gravitationally preferred rest frame [17]. The main effects produced if $\alpha_1 \neq 0$ are on the eccentricity vector $\mathbf{e}$ of the satellite's orbit [36] and on its mean argument of latitude $\ell_0 = \omega + M$, with ω the argument of pericenter and M the mean anomaly. In this Letter we focus on the effect of LLI violation on ℓ_0, that is a periodic effect with annual periodicity. From now on we will refer to ℓ_0 simply as the longitude of the satellite or observable. If LLI is violated, the Lagrangian $\mathcal{L}$ of the Earth-satellite system contains a perturbing term with the following explicit expression [17]:

$$\mathcal{L}_{\alpha_1} = -\frac{\alpha_1}{2c^2}\frac{G_N m_\oplus m_S}{r_{\oplus S}}(\mathbf{v}_\oplus + \mathbf{w}) \cdot (\mathbf{v}_S + \mathbf{v}_\oplus + \mathbf{w}), \quad (1)$$

where $m_\oplus$ and m_S are the mass of the Earth and of the satellite, while G_N, c and $r_{\oplus S}$ are, respectively, the Newtonian gravitational constant, the speed of light, and the distances between the two masses. In Eq. (1) $\mathbf{v}_\oplus$ is the velocity of the Earth with respect to the Sun, $\mathbf{w}$ is the "absolute" (i.e., with respect to the preferred frame) velocity of the Sun, and $\mathbf{v}_S$ is the orbital velocity of the satellite around the Earth. So, $\mathbf{v}_\oplus + \mathbf{w}$ represents the "absolute" velocity of the Earth while $\mathbf{v}_S + \mathbf{v}_\oplus + \mathbf{w}$ represents the "absolute" velocity of the satellite. The following two equations are the Lagrange's perturbation equations in the argument of pericenter and in the mean anomaly:

$$\frac{d\omega}{dt} = -\frac{\cos i}{na^2(1-e^2)^{1/2}\sin i}\frac{\partial\mathcal{R}}{\partial i} + \frac{(1-e^2)^{1/2}}{na^2 e}\frac{\partial\mathcal{R}}{\partial e}, \quad (2)$$

$$\frac{dM}{dt} = n - \frac{1-e^2}{na^2 e}\frac{\partial\mathcal{R}}{\partial e} - \frac{2}{na}\frac{\partial\mathcal{R}}{\partial a}, \quad (3)$$

where $\mathcal{R}$ is the disturbing function, which is obtained from the perturbing potential of the Lagrangian [37]. If we now add up the two rates to construct the observable $\dot{\ell}_0 = \dot{\omega} + \dot{M}$, the terms linked to $\partial\mathcal{R}/\partial e$ tend to cancel out, and this is truer the smaller the eccentricity e of the orbit. The advantage of considering the sum of the two observables of Eqs. (2) and (3), is that most of the perturbative effects of the main gravitational and nongravitational perturbations tend to be reduced on the final observable $\dot{\ell}_0$ [38]. By working out the dot product of Eq. (1), the disturbing function reduces to

$$\langle\mathcal{R}\rangle_{2\pi} = -\frac{\alpha_1}{c^2}\frac{G_N m_\oplus}{a}(\mathbf{w}\cdot\mathbf{v}_\oplus), \quad (4)$$

where the notation $\langle\mathcal{R}\rangle_{2\pi}$ implies that we take the average over the unperturbed two-body Keplerian orbit of the satellite around the Earth. We now insert this last expression into Eqs. (2) and (3), and only retain terms that contain $\partial\mathcal{R}/\partial a$ that are relevant for the effect we seek. Using Kepler's third law we finally obtain

$$\langle\dot{\ell}_0\rangle_{2\pi} = \langle\dot{\ell}_0\rangle_{2\pi}^{\mathrm{per}} - 2\alpha_1 n\frac{(\mathbf{w}\cdot\mathbf{v}_\oplus)}{c^2} + \mathcal{O}(e\alpha_1), \quad (5)$$

where the first term takes into account possible long-term periodic perturbative effects of both gravitational and nongravitational nature. To compute the term related to the PPN parameter α_1 we introduce the plane of the ecliptic as astronomical reference frame with the Sun at the origin, the direction $\hat{\mathbf{x}}$ toward the vernal equinox Υ and $\hat{\mathbf{z}}$ normal to the ecliptic plane. In this frame, the two velocities in Eq. (5) take the form (see Table I):

TABLE I. Solar-system velocity $\mathbf{w}$ with respect to the cosmic microwave background. Coordinates are in the ecliptic reference frame. The estimated errors are ±2 km/s and ±0°.01. Adapted from [2].

	Velocity vector $\mathbf{w}$
Absolute value: w	368 km/s
Latitude: β_{PF}	−11°.13
Longitude: λ_{PF}	171°.55

$$\mathbf{w} = w(\cos\beta_{PF}\cos\lambda_{PF}\hat{\mathbf{x}} + \cos\beta_{PF}\sin\lambda_{PF}\hat{\mathbf{y}} + \sin\beta_{PF}\hat{\mathbf{z}}), \tag{6}$$

$$\mathbf{v}_\oplus = v_\oplus(\sin(\lambda_0 + \dot{\lambda}_\oplus t)\hat{\mathbf{x}} - \cos(\lambda_0 + \dot{\lambda}_\oplus t)\hat{\mathbf{y}}). \tag{7}$$

In Eq. (6), the coordinates $(\beta_{PF}, \lambda_{PF})$ represent, respectively, the ecliptic latitude and longitude that identify the direction of the preferred frame (in this analysis, that of CMB radiation). In Eq. (7), λ_0 represents the ecliptic longitude of the Earth around the Sun at a fixed epoch, while $\dot{\lambda}_\oplus$ represents its angular orbital rate. This angular rate can be approximated with the Earth's mean motion $n_\oplus = \sqrt{G_N M_\odot / a^3_{\odot\oplus}}$, assuming for simplicity a circular Earth orbit (where $M_\odot$ and $a_{\odot\oplus}$ represent, respectively, the mass of the Sun and the astronomical unit). Substituting these expressions for the velocities $\mathbf{w}$ and $\mathbf{v}_\oplus$ into Eq. (5), we finally obtain

$$\langle \dot{\ell}_0 \rangle_{2\pi} = -2\alpha_1 n \frac{w v_\oplus}{c^2}\cos\beta_{PF}\sin(\lambda_0 + n_\oplus t - \lambda_{PF}) + \ldots, \tag{8}$$

where the dots represent minor contributions and we have temporarily removed the unmodeled or poorly modeled periodic effects.

Orbit determination and residuals—The precise orbit determination (POD) of the LAGEOS satellites has been made using two independent software packages, GEODYN II [40] and SATAN [41], for the data reduction of the satellite tracking data. The orbit analysis covers a time span of about 28.3 years, starting from October 31, 1992 (i.e., MJD 48925), in the case of GEODYN II POD, and about 31.4 years, starting from February 7, 1993 (i.e., MJD 49025), in the case of the POD conducted with SATAN. Figure 1 shows the results, in the case of LAGEOS, for the residuals in our observable $\dot{\ell}_0 = \dot{\omega} + \dot{M}$, introduced to set bounds on the α_1 parameter [42]. The black line represents the GEODYN II residuals, while the red line represents the residuals obtained with SATAN. These residuals represent the variation of the orbital longitude over 7 days: this is the duration of an "arc," and is the time unit of these measurements and of our analysis. The residuals contain the impact of unmodeled perturbing effects on the satellite's orbit [43].

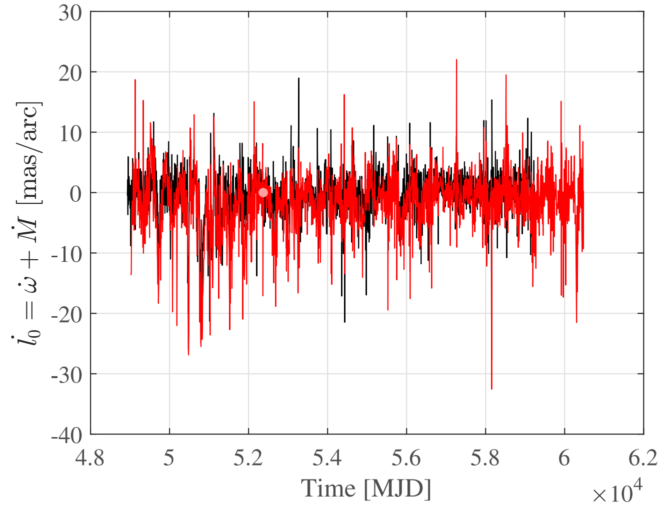

FIG. 1. LAGEOS seven-day residuals in the rate of the longitude $\ell_0 = \omega + M$ versus time (black: GEODYN II, red: SATAN).

The presence of the possible PFE on these residuals is, however, masked by a plethora of gravitational and non-gravitational effects of both periodic and secular nature. This is also shown in Fig. 2, that represents the frequency domain representation, via the fast Fourier transform (FFT), of the residuals of Fig. 1. We can take advantage of the two independent measurements of the longitudes ℓ_0 of the LAGEOS satellites to reduce the error in the measurement of the parameter α_1. As widely discussed in [16], the main systematic error on these observables is due to the imperfect knowledge of the Earth's quadrupole coefficient $\bar{C}_{2,0}$ used in the POD. Following Kozai [44], and

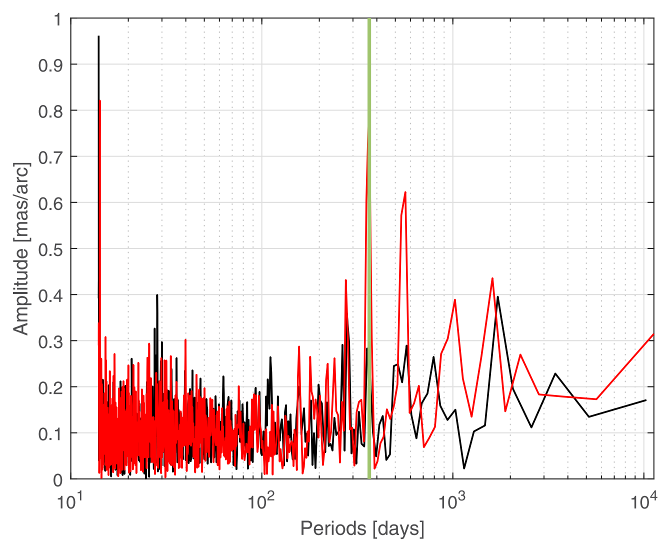

FIG. 2. FFT of the residuals in the rate of the longitude $\ell_0 = \omega + M$ of LAGEOS over the time span of the analysis. For ease of consultation, the plot abscissa represents the periods, i.e., 1/frequency. A peak at annual periodicity is clearly visible (black: GEODYN II, red: SATAN).

neglecting the contribution of the terms of $\mathcal{O}(e^2)$, we can relate the error $\delta\bar{C}_{2,0}$ with that of the longitude rate $\delta(\dot{\ell}_0)$:

$$\delta(\dot{\ell}_0)|_{\delta\bar{C}_{2,0}} \simeq \frac{3}{2}\sqrt{5}\left(\frac{R_\oplus}{a}\right)^2 n(3-4\sin^2 i)\delta\bar{C}_{2,0}. \quad (9)$$

By using equations (9) and (8) together, we can treat the longitudes $\dot{\ell}_0^{LG1}$ and $\dot{\ell}_0^{LG2}$ obtained by the PODs of LAGEOS and LAGEOS II as the left-hand sides in a linear system of two equations in two unknowns. The two unknowns are the variables $\delta\bar{C}_{2,0}$ and $A_1(t)$. The latter accounts for the possible contribution of α_1 at the annual frequency, decoupled from its primary systematic error, $\delta\bar{C}_{2,0}$. The system to solve is

$$\begin{aligned} \dot{\ell}_0^{LG1} &= K_1^{LG1}\,A_1(t) + K_2^{LG1}\,\delta\bar{C}_{2,0} \\ \dot{\ell}_0^{LG2} &= K_1^{LG2}\,A_1(t) + K_2^{LG2}\,\delta\bar{C}_{2,0} \end{aligned} \quad (10)$$

with K_1^{LG} and K_2^{LG} the coefficients multiplying α_1 and $\delta\bar{C}_{2,0}$ in Eqs. (8) and (9). We are interested in detecting a signal, related to our observable, that varies with annual period and with a well defined phase. To isolate this signal from the other frequency components, we adopt a phase-sensitive detection (PSD) scheme: a homodyne demodulation at the target frequency (the annual one) and phase, followed by a low-pass filter [45]. In this way we obtain the amplitude of the target signal as a function of time at zero frequency. In conclusion, applying the phase-sensitive detection to the solution $A_1(t)$ of the system (10), we finally obtain

$$\alpha_1 \simeq \langle \sin(n_\oplus t + \phi_0)A_1(t)\rangle_{2\pi}, \quad (11)$$

where $\phi_0 = \lambda_0 - \lambda_{PF}$. This DC component represents the possible violation signal to be extracted from the final data. In this regard, while the FFT of the residuals of Fig. 2 identifies prominent nonannual peaks in the proximity of the target frequency, they do not impact into the α_1 measurement channel. The most significant of these features are located at periods of approximately 280 days—with amplitudes of ∼18.3 mas/yr for GEODYN II and ∼22.4 mas/yr for SATAN—and 550 days, with amplitudes of ∼13.0 mas/yr and ∼31.3 mas/yr, respectively. The PSD pipeline effectively handles these off-annual signals by operating as an extremely narrow-band filter. Specifically, the combination of a 3000-day integration time and a third-order Butterworth low-pass filter (providing ∼60 dB/decade attenuation) ensures a detection bandwidth sharp enough to isolate the annual signature while suppressing any influence from nearby periodicities.

Measurement and constraint—The PSD technique was applied using a reference signal with annual frequency $f_0 \simeq 2.738 \times 10^{-3}$ days^{-1} and phase ϕ_0. The initial phase ϕ_0 was fixed for each analysis based on the Earth's ecliptic longitude λ_0 at the respective start dates: $\lambda_0 \simeq 223°.83$ required $\phi_0 = 52°.28$ and $\lambda_0 \simeq 318°.23$ required $\phi_0 = 146°.68$, respectively, for GEODYN II and SATAN. Figure 3 shows the results of the in-phase component of $A_1(t)$. The DC component estimated from this plot represents the value of α_1 and, therefore, of a possible violation of the LLI. Figure 3 also shows that PSD filtering has a settling time. To avoid ringing effects, we considered data from day 2000 to day 9000 for each analysis, within which we do not expect a signal altered by the low-pass filter. From the PSD output we computed the mean and standard deviation of the constrained parameter and obtained

$$\begin{aligned} \alpha_1 &= (+2 \pm 3) \times 10^{-5} \quad \textit{with}\ \text{GEODYN II} \\ \alpha_1 &= (+1 \pm 2) \times 10^{-5} \quad \textit{with}\ \text{SATAN}. \end{aligned} \quad (12)$$

These results are fully compatible with a null value for the PPN parameter. The robustness of the α_1 constraint was verified by varying the filter order between 3 and 5 and the integration time between 2000 and 5000 days, yielding consistent results. Figure 4 represents the estimate obtained for the parameter α_1 by further varying the phase of the (ideal) demodulation sinusoid: with $\phi = [0, 2\pi]$ while keeping the reference period at 365.25 days. The solid lines show how the PPN parameter estimate varies in the case of the in-phase analysis while the dashed line shows

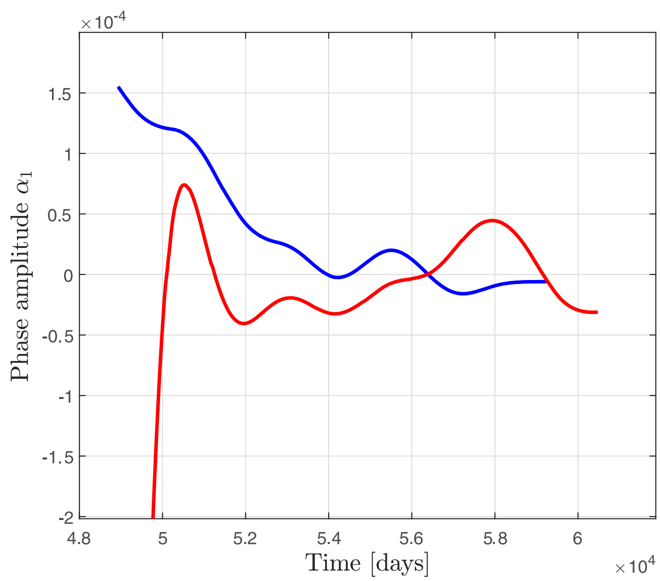

FIG. 3. Time behavior of $A_1(t)$ after the PSD for the in-phase analysis: blue: GEODYN II and red: SATAN. In this specific case we used a third-order low-pass filter, corresponding to an attenuation of about 60 dB per decade of the amplitude of the signal above the cutoff frequency. The low-pass filter removes the higher frequencies and leaves the long-term trend we are looking for. A value of 3000 days was assumed for the integration time of the low-pass filter.

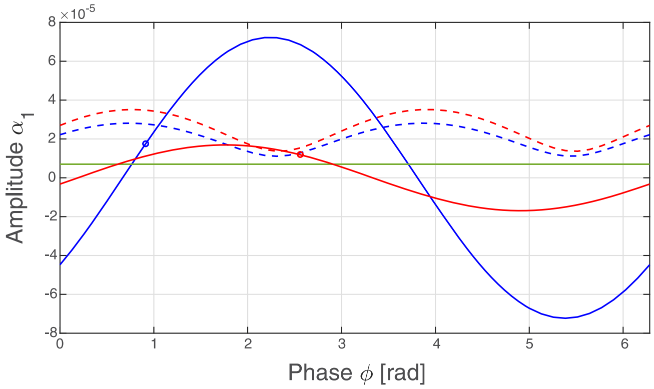

FIG. 4. Behavior of α_1 (solid line: blue: GEODYN II and red: SATAN) as the phase of the demodulation sinusoid varies. The frequency of the sinusoid is fixed at the annual value. The blue and red dashed lines represent the corresponding values for the standard deviation. The two circles, blue and red, correspond to the values of α_1 obtained for GEODYN II and SATAN, respectively; see Eq. (12). The green continuous line shows the overall estimated systematic error to α_1 due to both gravitational and nongravitational perturbations, about 8×10^{-6}. The filter parameters are the same as those used in Fig. 3.

the variation of the standard deviation in the same time interval of 7000 days. The values of α_1 at the phases $\phi = \phi_0 \simeq 0.91$ rad (blue circle) and $\phi = \phi_0 \simeq 2.56$ rad (red circle) correspond to the specific cases of Fig. 3. Both in the case of the GEODYN II and SATAN analyses, it is worth emphasizing that the maximum values of α_1 are not obtained at the phase $\phi = \phi_0$, but at a higher value equal to approximately 2.18 rad for GEODYN II, and at a lower value around 1.79 rad for SATAN. This reinforces our conclusion that what we obtain at the expected frequency and phase value for the violation actually represents a null measurement for the PPN parameter. In the figure, the horizontal green line represents the overall systematic error $\lesssim 8 \times 10^{-6}$ in the measurement of α_1, which we consider to be independent of the phase of the possible violation signal. A detailed study of the main systematic errors is reported in the companion paper [16]. The budget is dominated by the uncertainty in the Earth's hexadecapole coefficient $\bar{C}_{4,0}$, which contributes an error of $\sim 6.5 \times 10^{-6}$. To assess the impact of nongravitational perturbations (NGPs), we performed a rigorous end-to-end simulation, processing our high-fidelity NGP models through the entire measurement pipeline. This analysis confirms that the systematic bias from NGPs is negligible, with the largest contribution from SRP model errors being $(-0.4 \pm 4.0) \times 10^{-6}$. Table II summarizes the final error budget.

The detailed error budget described in [16] leads to three significant conclusions: (i) it underscores the thoroughness of our nongravitational force modeling, (ii) our analysis is demonstrably limited by statistics and not by systematics, and (iii) the statistical error is due to broadband noise

TABLE II. Systematic error budget for the α_1 measurement. The total systematic error is calculated as the root sum square (RSS) of individual contributions.

Error source	Systematic error ($\lvert\Delta\alpha_1\rvert$)
Gravitational ($\bar{C}_{4,0}$)	6.5×10^{-6}
Solar radiation pressure (SRP)	4.0×10^{-6}
Ocean tides	1.0×10^{-7}
Solid tides	1.0×10^{-9}
Thermal effects (YS/EY)	$4.0 \times 10^{-8}/1.0 \times 10^{-11}$
Total Systematic (RSS)	$\sigma_{\rm sys} \approx 7.7 \times 10^{-6}$
Statistical ($\sigma_{\rm stat}$): SATAN/GEODYN	$2 \times 10^{-5}/3 \times 10^{-5}$

around the annual period. Hence, the analysis of the systematic errors reinforces the conclusion of a measurement consistent with zero for α_1. Uncertainties in the CMB reference frame parameters (velocity w, latitude β_{PF}, and longitude λ_{PF}) propagate into a final uncertainty in α_1 of only $\sim 10^{-7}$, which is 2 orders of magnitude below our quoted statistical errors.

Conclusions—Local Lorentz invariance (LLI) is a cornerstone of both the standard model of particle physics and general relativity, and as such, it underpins our fundamental understanding of spacetime. Testing LLI is therefore a powerful probe for new physics. Many alternative theories of gravity introduce additional fields that can mediate the gravitational interaction, potentially violating LLI and giving rise to preferred-frame effects (PFE). In this Letter, we present a new test of LLI in the gravitational sector by searching for PFE in the orbits of the LAGEOS and LAGEOS II satellites. Our analysis spans nearly three decades of precise satellite laser ranging data and employs two independent orbit determination software for cross-validation. The constraint is derived from a phase-sensitive detection of an annual periodic effect in the orbital residuals of the satellites' mean argument of latitude. Using the POD software SATAN, we found $\alpha_1 = (+1 \pm 2) \times 10^{-5}$ for the parametrized post-Newtonian (PPN) parameter, while with GEODYN II we obtained a consistent result of $\alpha_1 = (+2 \pm 3) \times 10^{-5}$. The total systematic error budget is dominated by the uncertainty in the Earth's hexadecapole harmonic $\bar{C}_{4,0}$ and is estimated to be $\sigma_{\rm sys} \approx 8 \times 10^{-6}$, which is about 2 times smaller than the statistical uncertainty obtained with SATAN. This result is consistent with a null value for α_1, in full agreement with the predictions of general relativity. The robustness of this null result was further confirmed through extensive testing, detailed in [16]. An analysis of the data using a shorter lock-in integration time (500 days) produced a time series of nearly uncorrelated α_1 estimates that shows no significant temporal variation, confirming the stability of our result. Furthermore, an extreme sensitivity analysis demonstrated that our measurement is insensitive to large, pessimistic variations in key model parameters. This Letter provides the first constraint on the PPN parameter α_1 using satellite orbital data in the Earth's gravitational field. It improves upon the previous best constraint from lunar laser ranging [11] by more than a factor of 4, placing stringent new limits on the existence of a preferred frame for local gravitational physics and, consequently, on theories that feature additional vector or tensor fields, such as Einstein-aether theory [46,47]. In [16] we give the bounds on the parameter space and coupling constants of Einstein-aether theory and a detailed comparison of our result for α_1 with other tests of Lorentz invariance.

Acknowledgments—This work has been performed by the SaToR-G (Satellite Test of Relativistic Gravity) Collaboration funded by the Commissione Scientifica Nazionale 2 (CSN2) of the Istituto Nazionale di Fisica Nucleare (INFN), to which we are very grateful. The authors acknowledge the International Laser Ranging Service (ILRS) for providing high-quality laser ranging data of the LAGEOS and LAGEOS II satellites and an anonymous Referee for helpful comments and remarks that have considerably improved the original Letter. This work is partially supported by ICSC–Centro Nazionale di Ricerca in High Performance Computing, Big Data and Quantum Computing, funded by European Union–NextGenerationEU.

Data availability—The main data that support the findings of this article are openly available in the Zenodo repository at [49].

[1] A. Einstein, Die grundlage der allgemeinen relativitätstheorie, Ann. Phys. (Berlin) **354**, 769 (1916).
[2] C. M. Will, *Theory and Experiment in Gravitational Physics* (Cambridge University Press, Cambridge, England, 2018).
[3] T. Damour and G. Esposito-Farese, Tensor-multi-scalar theories of gravitation, Classical Quantum Gravity **9**, 2093 (1992).
[4] K. Nordtvedt, Equivalence principle for massive bodies. II. Theory, Phys. Rev. **169**, 1017 (1968).
[5] C. M. Will, Theoretical frameworks for testing relativistic gravity. II. Parametrized post-Newtonian hydrodynamics, and the Nordtvedt effect, Astrophys. J. **163**, 611 (1971).
[6] J. K. Nordtvedt and C. M. Will, Conservation laws and preferred frames in relativistic gravity. II. Experimental evidence to rule out preferred-frame theories of gravity, Astrophys. J. **177**, 775 (1972).
[7] C. M. Will and J. K. Nordtvedt, Conservation laws and preferred frames in relativistic gravity. I. Preferred-frame theories and an extended PPN formalism, Astrophys. J. **177**, 757 (1972).
[8] D. Mattingly, Modern tests of Lorentz invariance, Living Rev. Relativity **8**, 5 (2005).
[9] S. Liberati, Tests of Lorentz invariance: A 2013 update, Classical Quantum Gravity **30**, 133001 (2013).
[10] J. Müller, K. Nordtvedt, and D. Vokrouhlický, Improved constraint on the α_1 PPN parameter from lunar motion, Phys. Rev. D **54**, R5927 (1996).
[11] J. Müller, J. G. Williams, and S. G. Turyshev, Lunar Laser Ranging Contributions to Relativity and Geodesy, in *Lasers, Clocks and Drag-Free Control: Exploration of Relativistic Gravity in Space*, edited by H. Dittus, C. Lammerzahl, and S. G. Turyshev (Springer, Berlin, Heidelberg, 2008), pp. 457–472.
[12] P. L. Bender, D. G. Currie, R. H. Dicke, D. H. Eckhardt, J. E. Faller, W. M. Kaula, J. D. Mulholland, H. H. Plotkin, S. K. Poultney, E. C. Silverberg, D. T. Wilkinson, J. G. Williams, and C. O. Alley, The lunar laser ranging experiment, Science **182**, 229 (1973).
[13] K. Nordtvedt, Probing gravity to the second post-Newtonian order and to one part in 10^7 using the spin axis of the sun, Astrophys. J. **320**, 871 (1987).
[14] M. R. Pearlman, J. J. Degnan, and J. M. Bosworth, The international laser ranging service, Adv. Space Res. **30**, 135 (2002).
[15] M. R. Pearlman, C. E. Noll, E. C. Pavlis, F. G. Lemoine, L. Combrink, J. J. Degnan, G. Kirchner, and U. Schreiber, The ILRS: Approaching 20 years and planning for the future, J. Geodes. **93**, 2161 (2019).
[16] D. M. Lucchesi *et al.*, companion paper, Local Lorentz invariance test with the LAGEOS satellites, Phys. Rev. D **114**, 024072 (2026).
[17] T. Damour and G. Esposito-Farèse, Testing for preferred-frame effects in gravity with artificial Earth satellites, Phys. Rev. D **49**, 1693 (1994).
[18] C. W. Johnson, C. A. Lundquist, and J. L. Zurasky, Anaheim International Astronautical Federation Congress (1976).
[19] NASA, LAGEOS Phase B Technical Report, NASA Technical Memorandum X-64915, Technical Report TMX-64915 (Marshall Space Flight Center, Marshall Space Flight Center, Alabama 35812, 1975) february 1975.
[20] S. C. Cohen and D. E. Smith, Lageos scientific results—Introduction, J. Geophys. Res. **90**, 9217 (1985).
[21] F. Fontana, Physical properties of LAGEOS II satellite, Technical Report LG-TN-AI-037 (Aeritalia, 1989).
[22] Of course, it is necessary to develop a dynamic model for the orbit of these satellites that is equally reliable and accurate [23–26].
[23] D. Lucchesi, L. Anselmo, M. Bassan, C. Pardini, R. Peron, G. Pucacco, and M. Visco, Testing the gravitational interaction in the field of the Earth via satellite laser ranging and the Laser Ranged Satellites Experiment (LARASE), Classical Quantum Gravity **32**, 155012 (2015).
[24] D. M. Lucchesi, L. Anselmo, M. Bassan, C. Magnafico, C. Pardini, R. Peron, G. Pucacco, and M. Visco, General relativity measurements in the field of Earth with laser-ranged satellites: State of the art and perspectives, Universe **5**, 141 (2019).
[25] M. Visco and D. M. Lucchesi, Review and critical analysis of mass and moments of inertia of the LAGEOS and LAGEOS II satellites for the LARASE program, Adv. Space Res. **57**, 1928 (2016).
[26] M. Visco and D. M. Lucchesi, Comprehensive model for the spin evolution of the LAGEOS and LARES satellites, Phys. Rev. D **98**, 044034 (2018).

[27] I. Ciufolini, D. Lucchesi, F. Vespe, and A. Mandiello, Measurement of dragging of inertial frames and gravitomagnetic field using laser-ranged satellites, Nuovo Cimento Soc. Ital. Fis. **109A**, 575 (1996).

[28] I. Ciufolini and E. C. Pavlis, A confirmation of the general relativistic prediction of the Lense-Thirring effect, Nature (London) **431**, 958 (2004).

[29] D. M. Lucchesi, The Lense-Thirring effect derivation and the LAGEOS satellites orbit analysis with the new gravity field solution from CHAMP, in *35th COSPAR Scientific Assembly*, COSPAR Meeting, edited by J.-P. Paillé (2004), Vol. 35, p. 232, https://ui.adsabs.harvard.edu/abs/2004cosp..35..232L/abstract.

[30] D. M. Lucchesi and R. Peron, Accurate measurement in the field of the Earth of the general-relativistic precession of the LAGEOS II Pericenter and new constraints on non-Newtonian gravity, Phys. Rev. Lett. **105**, 231103 (2010).

[31] D. M. Lucchesi and R. Peron, LAGEOS II pericenter general relativistic precession (1993-2005): Error budget and constraints in gravitational physics, Phys. Rev. D **89**, 082002 (2014).

[32] D. M. Lucchesi, M. Visco, R. Peron, M. Bassan, G. Pucacco, C. Pardini, L. Anselmo, and C. Magnafico, An improved measurement of the Lense-Thirring precession on the orbits of laser-ranged satellites with an accuracy approaching the 1% level, arXiv:1910.01941.

[33] I. Ciufolini, A. Paolozzi, E. C. Pavlis, G. Sindoni, J. Ries, R. Matzner, R. Koenig, C. Paris, V. Gurzadyan, and R. Penrose, An improved test of the general relativistic effect of frame-dragging using the LARES and LAGEOS satellites, Eur. Phys. J. C **79**, 872 (2019).

[34] D. Lucchesi, M. Visco, R. Peron, M. Bassan, G. Pucacco, C. Pardini, L. Anselmo, and C. Magnafico, A 1% Measurement of the gravitomagnetic field of the Earth with laser-tracked satellites, Universe **6**, 139 (2020).

[35] D. Lucchesi, L. Anselmo, M. Bassan, M. Lucente, C. Magnafico, C. Pardini, R. Peron, G. Pucacco, and M. Visco, Testing gravitational theories in the field of the Earth with the SaToR-G experiment, Universe **7**, 192 (2021).

[36] This is the Laplace-Runge-Lenz vector that identifies the satellite pericenter direction: A constant of motion in the ideal case of the 2-body Newtonian problem.

[37] To compute the variation of the orbital elements, a linear perturbation approach is sufficient in which the right-hand sides of the above perturbing equations are evaluated by keeping constant, to their (mean) nominal values, the semimajor axis a, the eccentricity e, the inclination i, and the mean motion $n = \sqrt{G_N m_\oplus / a^3}$.

[38] This is also true in the case of some relativistic effects, such as Schwarzschild precession [39].

[39] M. H. Soffel and W.-B. Han, *Applied General Relativity* (Springer, Cham, 2019).

[40] D. E. Pavlis *et al.*, GEODYN II Operations Manual, NASA GSFC (1998).

[41] A. T. Sinclair and G. M. Appleby, SATAN: Programs for the determination and analysis of satellite orbits for SLR data, Technical Report, 1988.

[42] These residuals were obtained by adding the residuals in the rate of the argument of pericenter and in the rate of the mean anomaly of LAGEOS (see Fig. 1 in [16]), after removing, on the basis of the rates reported in Table IV of the same paper, the total relativistic precession predicted by GR (not modeled in the POD) on the rates of the argument of pericenter and of the mean anomaly.

[43] The overall period of our analysis has been divided into seven-day arcs not causally connected to each other, and the initial state vector for each arc has been adjusted in the POD procedure to best fit the tracking data.

[44] Y. Kozai, The motion of a close Earth satellite, Astron. J. **64**, 367 (1959).

[45] The periodic signal that we wish to detect, after the homodyne detection, splits into a DC component and a periodic component with a frequency double that of the initial one, and both components with an amplitude half of the initial one. This signal is low-pass filtered for the final analysis and measurement.

[46] T. Jacobson and D. Mattingly, Einstein-aether waves, Phys. Rev. D **70**, 024003 (2004).

[47] We note that Einstein-aether theory can be regarded as the low-energy limit of Hořava-Lifshitz gravity [48].

[48] P. Hořava, Spectral dimension of the universe in quantum gravity at a Lifshitz point, Phys. Rev. Lett. **102**, 161301 (2009).

[49] https://zenodo.org/records/18441938.